Published in final edited form as:
Dev Cell. 2008 July ; 15(1): 163–169. doi:10.1016/j.devcel.2008.05.016.

Myosin II Activity Facilitates Microtubule Bundling in the Neuronal Growth Cone Neck

Dylan T. Burnette[1], **Lin Ji**[2], **Andrew W. Schaefer**[1], **Nelson A. Medeiros**[1], **Gaudenz Danuser**[2], and **Paul Forscher**[1,*]

1*Department of Molecular, Cellular and Developmental Biology, Yale University, New Haven, CT 06511, USA*

2*Dept of Cell Biology, The Scripps Research Institute (TSRI), La Jolla, CA 92037, USA*

SUMMARY

The cell biological processes underlying axon growth and guidance are still not well understood. An outstanding question is how a new segment of the axon shaft is formed in the wake of neuronal growth cone advance. For this to occur, the highly dynamic, splayed-out microtubule (MT) arrays characteristic of the growth cone must be consolidated (bundled together) to form the core of the axon shaft. MT-associated proteins stabilize bundled MTs, but how individual MTs are brought together for initial bundling is unknown. Here, we show that laterally moving actin arcs, which are myosin II-driven contractile structures, interact with growing MTs and transport them from the sides of the growth cone into the central domain. Upon Myosin II inhibition, the movement of actin filaments and MTs immediately stopped and MTs unbundled. Thus, Myosin II-dependent compressive force is necessary for normal MT bundling in the growth cone neck.

INTRODUCTION

Growth cones are highly motile sensory structures that regulate the rate and direction of neurite advance during neuronal development and nerve regeneration. As growth cones move forward, a new segment of neurite shaft is generated by a process that encompasses three discrete morphological phases (reviewed in Dent and Gertler, 2003). Phase 1 is “protrusion” of the growth cone’s leading edge, a flat actin filament (F-actin)-rich lamellar region called the peripheral (P) domain. Phase 2 is “engorgement” of the central (C) domain characterized by advance of organelles and associated-microtubules (MTs). In Phase 3, the spread organelles and MTs are “consolidated” at the growth cone neck into a compact, stable new segment of the neurite shaft. These steps were first described using differential interference contrast (DIC) time-lapse microscopy (Goldberg and Burmeister, 1986) and have become the basis of modern axon growth models. Despite much recent investigation and progress in understanding F-actin-based protrusion at the leading edge (Pollard and Borisy, 2003), basic cytoskeletal mechanisms underlying the engorgement and consolidation phases of neurite growth remain poorly understood.

Evidence suggests MTs in the C domain are sequentially bundled together and stabilized during the consolidation process. MT bundling is thought to involve crosslinking by MT-associated proteins (MAPs), and MAPs have recently been shown to be necessary for consolidation (Bielas et al., 2007); however, how MTs are physically brought together to facilitate bundling

*Correspondence: E-mail: paul.forscher@yale.edu.

in the growth cone neck is unknown. To investigate this problem, we used a combination of fluorescent speckle microscopy (FSM), automated cytoskeletal flow tracking, and electron microscopy to characterize dynamic interactions between the actin filaments and MTs in the growth cone neck. We describe an actin/myosin II contractile system in this region that transports MTs from the sides of the growth cone and packs them into the C domain. We propose that this active MT transport facilitates MT bundling involved in formation of a new segment of axon shaft.

RESULTS

MT and Actin Filament Organization in the Growth Cone Neck

We used electron microscopy of *Aplysia* bag cell neurons treated with gold-labeled antibodies and prepared by rotary shadowing (Schaefer et al., 2002; Svitkina and Borisy, 1998) to investigate possible MT and F-actin interactions in the growth cone neck. Growth cones imaged with DIC or low-magnification EM showed similar structural organization (Figures 1A and 1B). Bundled MTs, visualized by immunogold labeling, were evident in the neurite shaft and growth cone neck (Figure 1C, arrow and circle, respectively). At higher magnification, a dendritic actin filament network on the sides of the neck (Figure 1D, star) and actin filament bundles in adjacent central regions (Figure 1D, arrow) were evident. MTs and actin filaments were pseudocolored to facilitate comparison of the two networks. The original gray-scale image is shown in Figure S1 (available online). Individual MT tips were detectable in lateral regions of the neck and these MTs were typically aligned with actin filament bundles (Figure 1D, arrowhead). MT density was high in central neck regions, making identification of MT tips or visualization of actin filaments difficult. However, fluorescence microscopy studies do indicate the presence of actin filaments in this region (Loudon et al., 2006; Zhang et al., 2003), consistent with MTs lying on top of, and obscuring, actin filament structures.

To further address this issue, the 3D organization of the actin and MT cytoskeleton in the neck region was visualized by spinning disk confocal microscopy. Figures 1E and 1F show through-focus merged image stacks for actin filaments and MTs. When cross sectional x–z sections in the growth cone neck were examined, an actin filament-dense “node” was present in the neck in 53.5% of growth cones (n = 258 growth cones) consistent with previous reports (Figure 1I, open arrowhead). In individual z sections, the bottom (ventral) section typically had markedly less MT labeling than the top (dorsal) section (Figures 1G and 1H, arrows). Together, these results suggest MTs tend to sit on top of actin filaments in the node region, and x–z scans from double-labeled preparations confirmed this was indeed the case (Figure 1I, cf. arrowheads).

Coordinated MT and Actin Filament Movement in the Growth Cone Neck

MT translocation and guidance by F-actin structures is an emerging theme in cell motility (Rodriguez et al., 2003). Indeed, the close MT-actin filament interactions observed (Figure 1) suggested MT movement in the growth cone neck might result from association with moving actin bundles. To test this hypothesis, Alexa-488 phalloidin and Alexa-594 tubulin were coinjected into neurons to visualize F-actin and MT dynamics (Figure 2) using total internal reflection fluorescence (TIRF) microscopy. To obtain slightly deeper fluorescence excitation cross sections, subcritical angles of TIRF laser incidence were used (Burmeister et al., 1994). This technique facilitated visualization and quantitative comparison of F-actin and MT movements in the thicker midsection of the growth cone neck (Figure 2). Filopodial actin bundles in the P- domain and actin arcs in the T zone are indicated by arrows and arrowheads, respectively (Schaefer et al., 2002). Actin arcs have previously been shown to be actin/myosin II contractile structures that form from condensation of dendritic actin networks in the T zone (Medeiros et al., 2006; Zhang et al., 2003). After formation, actin arcs moved into the C domain, merging into thicker actin bundles that tended to move toward a contractile node (Figure 2,

CN, yellow circle) situated in the growth cone neck. Actin arcs also form in the growth cone neck region (Figure S2), consistent with the dendritic actin networks and actin bundles visualized by EM in the same region (Figure 1).

Preliminary results suggested actin arcs could transport MTs and influence MT assembly dynamics (Schaefer et al., 2002; Zhang et al., 2003). To further investigate MT-actin interactions in the growth cone neck, we used newly developed cross correlation speckle tracking algorithms (Hu et al., 2007; Ji and Danuser, 2005) capable of calculating the direction and speed of every speckle in the image over successive sampling intervals. The resulting vectors, color coded according to speed, represent a quantitative map of actin filament flow (Figures 2C and 2D). Rates and patterns of classical retrograde actin flow in the P domain and actin arc translocation in the T zone measured by speckle tracking were similar to those previously reported (Medeiros et al., 2006; Schaefer et al., 2002; Zhang et al., 2003). In growth cone neck regions, actin filament bundles moved initially from the cell edge into the C domain and then proceeded toward the contractile node at 1–2 μm/min (Figure 2C, box). Interestingly, F-actin flow vectors formed an inward pointing radial array centered on the contractile node (Figure 2E). Comparison of actin filament and MT flow maps in the node region revealed similar flow patterns, consistent with actin filaments transporting MTs (Figure 2E versus 2F).

We next explored how MTs enter the growth cone. Detailed analysis of MT dynamics was only possible on the sides of the growth cone neck where the relatively low MT density facilitated unambiguous MT speckle tracking (Figure S3 and Table S1). Speckle analysis revealed that single MTs entered the sides of the growth cone via polymerization at rates of ~3.9 μm/min (Table S1, Figure S3B, and Movie S1). Damping MT assembly with taxol (Suter et al., 2004) resulted in rapid MT depletion (Figures S3D–S3G), consistent with a key role for MT assembly in their extension in this region. Overall, MTs spent 62.6% of the time growing versus 35.5% of the time in paused states (Table S1). Remarkably, only one MT catastrophe was observed in these experiments, which was immediately followed by a rescue event. As MTs entered the sides of the growth cone, they concurrently moved laterally into the C domain (kymograph, Figure S3C) in accord with the MT movements shown in the flow maps above (Figure 2F, see also Movie S1).

Myosin II Regulates Actin Dynamics in the Growth Cone Neck

The observations above suggested that actin/myosin II structures derived from actin arcs could be transporting MTs growing along the sides of the growth cone into the C domain. Consistent with this, previous reports have localized myosin II to the T zone and C domain (Loudon et al., 2006; Rochlin et al., 1995). Interestingly, in addition to its typical localization in the distal T zone (Figures 3A and 3B, green arrowheads) we found accumulation of myosin II in the contractile node region (Figures 3A and 3B, yellow arrowheads). These results suggested a potential role for myosin II in driving actin filament and MT movements in the growth cone neck.

To test this, we assessed the effects of the specific nonmuscle myosin II ATPase inhibitor blebbistatin (Straight et al., 2003; Medeiros et al., 2006) on actin filament dynamics in the neck region. Inspection of flow maps revealed a slow but persistent actin filament flow into the growth cone neck under control conditions (Figure 3E); in contrast, flow was much slower and significantly more random after blebbistatin treatment (Figure 3H). To quantify randomness, we assessed coherence of actin flow (Figure 3I) over time from the entire flow map. Coherence of flow is a measure of the degree of directional similarity in a population of speckle movements (Hu et al., 2007). Flow coherency dropped significantly from 0.93 ± 0.02 in controls to 0.31 ± 0.05 after blebbistatin treatment. Measurements taken from kymographs indicated nearly complete loss of flow after myosin II inhibition (Figure 3J, lines 1 and 2, versus Figure 3K,

lines 3 and 4) similar to effects on distal actin arcs (Medeiros et al., 2006), suggesting a common dependence on myosin II motor activity.

Blebbistatin effects on actin flow in the growth cone neck were accompanied by significant spreading of the C domain and associated organelles (Bridgman et al., 1986; Figures 3C, 3F, and 3L). However, spreading was never observed in more proximal regions of the neurite shaft, suggesting these regions had undergone some kind of stabilization (Figure 3L).

Myosin II Regulates MT Transport and Bundling in the Growth Cone Neck

The effects on C domain structure above suggested myosin II activity could be affecting MT distribution and/or dynamics. To address these issues, we used FSM and speckle tracking to assess MT dynamics before and after blebbistatin treatment. Simultaneous assessment of actin dynamics with a second fluorescent channel was impractical because blue light photoinactivates blebbistatin (Sakamoto et al., 2005).

We found MTs and associated organelles in the C domain spread out immediately after myosin II inhibition (Figures 4A–4D, Movie S2). Analysis of flow revealed the inward movement of MTs on the sides of the growth cone (Figures 4E and 4F) was completely suppressed in blebbistatin (Figure 4G). Indeed, MTs actually reversed direction and began to move outward toward the growth cone edge as the C domain expanded (Figure 4H). Unlike actin filaments, MT flow coherence was not significantly affected by blebbistatin treatment (0.90 ± 0.05 and 0.87 ± 0.05, control and blebbistatin, respectively). MT kymography was used to independently verify the results of the flow maps (Figure 4I, line 1 versus 3 and line 2 versus 4). New MT traces were detected after blebbistatin addition, indicating MTs were still extending past the kymograph reference line (Figure 4I, yellow arrowheads). MT assembly dynamics were not affected by blebbistatin treatment (Table S1). These results suggest that the outward MT spread observed in blebbistatin is driven by a directed force. An obvious possibility is that MT arrays are relaxing from a compressed state normally maintained by myosin II-dependent inward transport. Interestingly, MTs in the C domain appear to unbundle in the absence of myosin II activity.

DISCUSSION

Actin arcs form from condensation of dendritic actin networks in the transition zone (Zhang et al., 2003), where their myosin II-dependent contractility is essential for severing actin bundles associated with filopodium roots (Medeiros et al., 2006). Evidence presented in the current study suggests that myosin II contractility also plays a key role in regulating the shape and structure of the C domain. Specifically, actin bundles derived from actin arcs interact with MTs on the sides of the growth cone and transport them into the C domain (Figure 4, Movie S1). The resulting inward MT transport appears to place active constraints on C domain as follows. MTs are normally compressed during bundling (Figure 4, Movie S2). Constantly applied compression appears to be necessary for maintaining the structure of the growth cone neck, since MTs here spread out and unbundle after myosin II inhibition. This finding suggests that MTs in the C domain are not yet stably crosslinked. We speculate that MTs held in close proximity by actin/myosin II contractility may facilitate crosslinking by MAPs in the growth cone neck. The latter process in turn promotes generation of the stable “consolidated” MT arrays characteristic of the neurite shaft, which we found to be morphologically unaffected by myosin II inhibition (Figure S4).

Myosin II has been widely implicated as an effector in neurite retraction (Gallo, 2006; Gallo and Letourneau, 2004; Wylie and Chantler, 2003; Zhang et al., 2003). In addition, several repulsive cues thought to be involved in inhibition of nerve regeneration increase Myosin II activity through Rho→ROCK signaling. Indeed, inhibition of this pathway is being explored

in therapeutic contexts; for example, application of the pharmacological ROCK inhibitor Y-27632 or the Rho inhibitor C3 quantitatively improved nerve regeneration in animal models (Fournier et al., 2003; Lehmann et al., 1999). Previously, we presented evidence that contractile actin bundles in the C domain mediate Rho/ROCK/Myosin II-dependent neurite retraction (Zhang et al., 2003). In these studies, we noted that MTs in the C domain were more splayed out after Rho Kinase (ROCK) inhibition, consistent with the role we propose here for Myosin II in MT transport and bundling. These and related observations (Loudon et al., 2006; Turney and Bridgman, 2005) suggest that Rho/ROCK inhibition, while permitting or even promoting axon growth, could also result in guidance deficits. Indeed, in a related study (Schaefer et al., 2008, in this issue), we found that, ROCK inhibition had two separate effects on stimulus evoked neurite growth. First, growth responses occurred with a shorter delay, consistent with reduction of a barrier to neurite advance. Second, MT transport and bundling in the growth cone neck were compromised. These findings are consistent with ROCK and downstream myosin II activity regulating MT bundling during neurite shaft consolidation.

EXPERIMENTAL PROCEDURES

Cell Culture and Chemicals

Primary cultures of *Aplysia* bag cell neurons on poly-D-lysine-coated cover-slips were prepared as previously described (Forscher and Smith, 1988). DMSO, phalloidin, and TRITC-phalloidin were from Sigma-Aldrich; Alexa-594 phalloidin, and Alexa-488 phalloidin were from Molecular Probes; Blebbistatin and taxol were from Calbiochem. Bovine brain α/β tubulin dimers were labeled with Alexa-594 (Molecular Probes) as previously described (Zhang et al., 2003).

Immunocytochemistry

Localization of F-actin and MTs was as previously described (Forscher and Smith, 1988; Schaefer et al., 2002). Briefly, cells were fixed with 3.7% formaldehyde followed by extraction with 1% Triton X-100. Alexa-594 phalloidin was used to label F-actin. For MT labeling, mouse mAb clone B-5-1-2 (Sigma-Aldrich) was used with an Alexa-488 goat anti-mouse secondary (Molecular Probes). Z-section image stacks were acquired with a Perkin-Elmer Ultraview RS spinning disk confocal attached to an Olympus IX71 inverted microscope with a Hamamatsu cooled CCD camera and Ultraview software.

Live cell extractions were preformed as previously described (Schaefer et al., 2002) with modifications. Extraction with 1% Triton X-100 in cytoskeleton stabilization buffer (artificial salt water, 4% PEG, 1 μM TRITC-phalloidin, 10 μM Taxol, 5 μM EGTA, and 5 μM MgCl2) was followed by washing with wash buffer (BRIG 40, 1 μM TRITC phalloidin, 1 μM Taxol, 5 μM EGTA, 1 μM $MgCl^2$). Cells were then fixed with 3.7% formaldehyde. For myosin II localization, an *Aplysia* myosin II-specific rabbit antibody with an Alexa-488 goat anti-rabbit secondary (Molecular Probes) was used as previously described (Medeiros et al., 2006). Images were acquired using a Nikon Eclipse TE300 microscope with a Coolsnap HQ cooled CCD camera (Roper Scienctific) and Metamorph software (Universal Imaging).

Electron Microscopy

Electron microscopy of cells treated with gold-labeled antibodies was performed as previously described with modifications (Svitkina and Borisy, 1998). Briefly, cells were extracted with 1% Triton X-100 in cytoskeleton stabilization buffer (artificial salt water, 4% PEG, 10 μM phalloidin, 10 μM Taxol, 5 μM EGTA, 5 μM $MgCl^2$, and 10 mg/ml BAPTA). Cells were washed with wash buffer and then fixed with 2% glutaraldehyde for 20 min. Samples were washed three times (5 min each) with water followed by quenching with 20 mM Glycine (twice for 10 min each). For MT labeling, samples were incubated with mouse mAb clone B-5-1-2

(Sigma-Aldrich) for 1 hr in PBS, then washed with PBS. Next, goat anti-mouse secondary antibodies attached to 15 nm gold particles (Electron Microscopy Sciences) were applied to the samples in the following buffer overnight: 10 mM Tris, 0.5 M NaCl, and 0.05% Tween 20. Samples were washed three times and then fixed with 2% glutaraldehyde for 20 min followed by 2% tannic acid and 0.1% uranyl acetate for 20 min each. Samples were dehydrated in increasing concentrations of ethanol and critical point dried. Platinum/palladium rotary shadowing was followed by carbon shadowing. Replicas were mounted on formvar-coated EM grids and observed with transmission EM at 80 kV.

Multimode Fluorescent Speckle Microscopy

Microinjection of bag cell neurons was as previously described (Schaefer et al., 2002) with Alexa-488 or Alexa-594 Phalloidin (Molecular Probes) or Alexa-594 (Molecular Probes) labeled tubulin dimers. Actin and MT dynamics were assessed by total internal reflection (TIRF) speckle microscopy or variable angle (VA) TIRF microscopy. Multimode time-lapse microscopy was as previously described. Images were acquired using 10 or 5 s intervals with 300–600 ms integration times for fluorescent probes and 75 ms for DIC using a Coolsnap HQ or Cascade 512B cooled CCD camera (Roper Scientific). FSM was performed with a Nikon Eclipse 2000U multimode TIRF microscope.

Either kymography or an adaptive multiframe correlation approach was used as described previously to track the motion of fluorescently labeled phalloidin or MTs from unprocessed data (Ji and Danuser, 2005; Schaefer et al., 2002). For display, the contrast of F-actin FSM images was enhanced by processing with the following spatial filters: unsharp mask followed by low pass. For MT FSM analysis, contrast of the MT speckles was enhanced by processing as described (Schaefer et al., 2002). MT fluorescent images were processed with the following spatial filters: unsharp mask, low pass, Laplace edge enhancement, and a final low pass. Stacks of time-lapse images were converted into movies, time-lapse montages, and kymographs for analysis. Data are expressed as mean ± SEM unless otherwise stated. Statistical analysis was done with two-tailed paired t test.

Supplementary Material

Refer to Web version on PubMed Central for supplementary material.

ACKNOWLEDGMENTS

The authors would like to thank members of the Forscher lab for helpful comments and discussion. This work was supported by NIH grants RO1-NS28695 and RO1-NS051786 to P.F. and the Nikon Partners-in-Research Program.

REFERENCES

Bielas SL, Serneo FF, Chechlacz M, Deerinck TJ, Perkins GA, Allen PB, Ellisman MH, Gleeson JG. Spinophilin facilitates dephosphorylation of doublecortin by PP1 to mediate microtubule bundling at the axonal wrist. Cell 2007;129:579–591. [PubMed: 17482550]

Bridgman PC, Kachar B, Reese TS. The structure of cytoplasm in directly frozen cultured cells. II. Cytoplasmic domains associated with organelle movements. J. Cell Biol 1986;102:1510–1521. [PubMed: 3514635]

Burmeister JS, Truskey GA, Reichert WM. Quantitative analysis of variable-angle total internal reflection fluorescence microscopy (VA-TIRFM) of cell/substrate contacts. J. Microsc 1994;173:39–51. [PubMed: 8120882]

Dent EW, Gertler FB. Cytoskeletal dynamics and transport in growth cone motility and axon guidance. Neuron 2003;40:209–227. [PubMed: 14556705]

Forscher P, Smith SJ. Actions of cytochalasins on the organization of actin filaments and microtubules in a neuronal growth cone. J. Cell Biol 1988;107:1505–1516. [PubMed: 3170637]

Fournier AE, Takizawa BT, Strittmatter SM. Rho kinase inhibition enhances axonal regeneration in the injured CNS. J. Neurosci 2003;23:1416–1423. [PubMed: 12598630]

Gallo G. RhoA-kinase coordinates F-actin organization and myosin II activity during semaphorin-3A-induced axon retraction. J. Cell Sci 2006;119:3413–3423. [PubMed: 16899819]

Gallo G, Letourneau PC. Regulation of growth cone actin filaments by guidance cues. J. Neurobiol 2004;58:92–102. [PubMed: 14598373]

Goldberg DJ, Burmeister DW. Stages in axon formation: observations of growth of Aplysia axons in culture using video-enhanced contrast-differential interference contrast microscopy. J. Cell Biol 1986;103:1921–1931. [PubMed: 3782290]

Hu K, Ji L, Applegate KT, Danuser G, Waterman-Storer CM. Differential transmission of actin motion within focal adhesions. Science 2007;315:111–115. [PubMed: 17204653]

Ji L, Danuser G. Tracking quasi-stationary flow of weak fluorescent signals by adaptive multi-frame correlation. J. Microsc 2005;220:150–167. [PubMed: 16363999]

Lehmann M, Fournier A, Selles-Navarro I, Dergham P, Sebok A, Leclerc N, Tigyi G, McKerracher L. Inactivation of Rho signaling pathway promotes CNS axon regeneration. J. Neurosci 1999;19:7537–7547. [PubMed: 10460260]

Loudon RP, Silver LD, Yee HF Jr, Gallo G. RhoA-kinase and myosin II are required for the maintenance of growth cone polarity and guidance by nerve growth factor. J. Neurobiol 2006;66:847–867. [PubMed: 16673385]

Medeiros NA, Burnette DT, Forscher P. Myosin II functions in actin-bundle turnover in neuronal growth cones. Nat. Cell Biol 2006;8:215–226. [PubMed: 16501565]

Pollard TD, Borisy GG. Cellular motility driven by assembly and disassembly of actin filaments. Cell 2003;112:453–465. [PubMed: 12600310]

Rochlin MW, Itoh K, Adelstein RS, Bridgman PC. Localization of myosin II A and B isoforms in cultured neurons. J. Cell Sci 1995;108:3661–3670. [PubMed: 8719872]

Rodriguez OC, Schaefer AW, Mandato CA, Forscher P, Bement WM, Waterman-Storer CM. Conserved microtubule-actin interactions in cell movement and morphogenesis. Nat. Cell Biol 2003;5:599–609. [PubMed: 12833063]

Sakamoto T, Limouze J, Combs CA, Straight AF, Sellers JR. Blebbistatin, a myosin II inhibitor, is photoinactivated by blue light. Biochemistry 2005;44:584–588. [PubMed: 15641783]

Schaefer AW, Kabir N, Forscher P. Filopodia and actin arcs guide the assembly and transport of two populations of microtubules with unique dynamic parameters in neuronal growth cones. J. Cell Biol 2002;158:139–152. [PubMed: 12105186]

Schaefer AW, Schoonderwoert VThG, Lin J, Medeiros N, Danuser G, Forscher P. Coordination of acting filament and microtubule dynamics during neurite outgrowth. Dev. Cell 2008;15:146–162. [PubMed: 18606148]this issue

Straight AF, Cheung A, Limouze J, Chen I, Westwood NJ, Sellers JR, Mitchison TJ. Dissecting temporal and spatial control of cytokinesis with a myosin II Inhibitor. Science 2003;299:1743–1747. [PubMed: 12637748]

Suter DM, Schaefer AW, Forscher P. Microtubule dynamics are necessary for SRC family kinase-dependent growth cone steering. Curr. Biol 2004;14:1194–1199. [PubMed: 15242617]

Svitkina TM, Borisy GG. Correlative light and electron microscopy of the cytoskeleton of cultured cells. Methods Enzymol 1998;298:570–592. [PubMed: 9751908]

Turney SG, Bridgman PC. Laminin stimulates and guides axonal outgrowth via growth cone myosin II activity. Nat. Neurosci 2005;8:717–719. [PubMed: 15880105]

Wylie SR, Chantler PD. Myosin IIA drives neurite retraction. Mol. Biol. Cell 2003;14:4654–4666. [PubMed: 12960431]

Zhang XF, Schaefer AW, Burnette DT, Schoonderwoert VT, Forscher P. Rho-dependent contractile responses in the neuronal growth cone are independent of classical peripheral retrograde actin flow. Neuron 2003;40:931–944. [PubMed: 14659092]

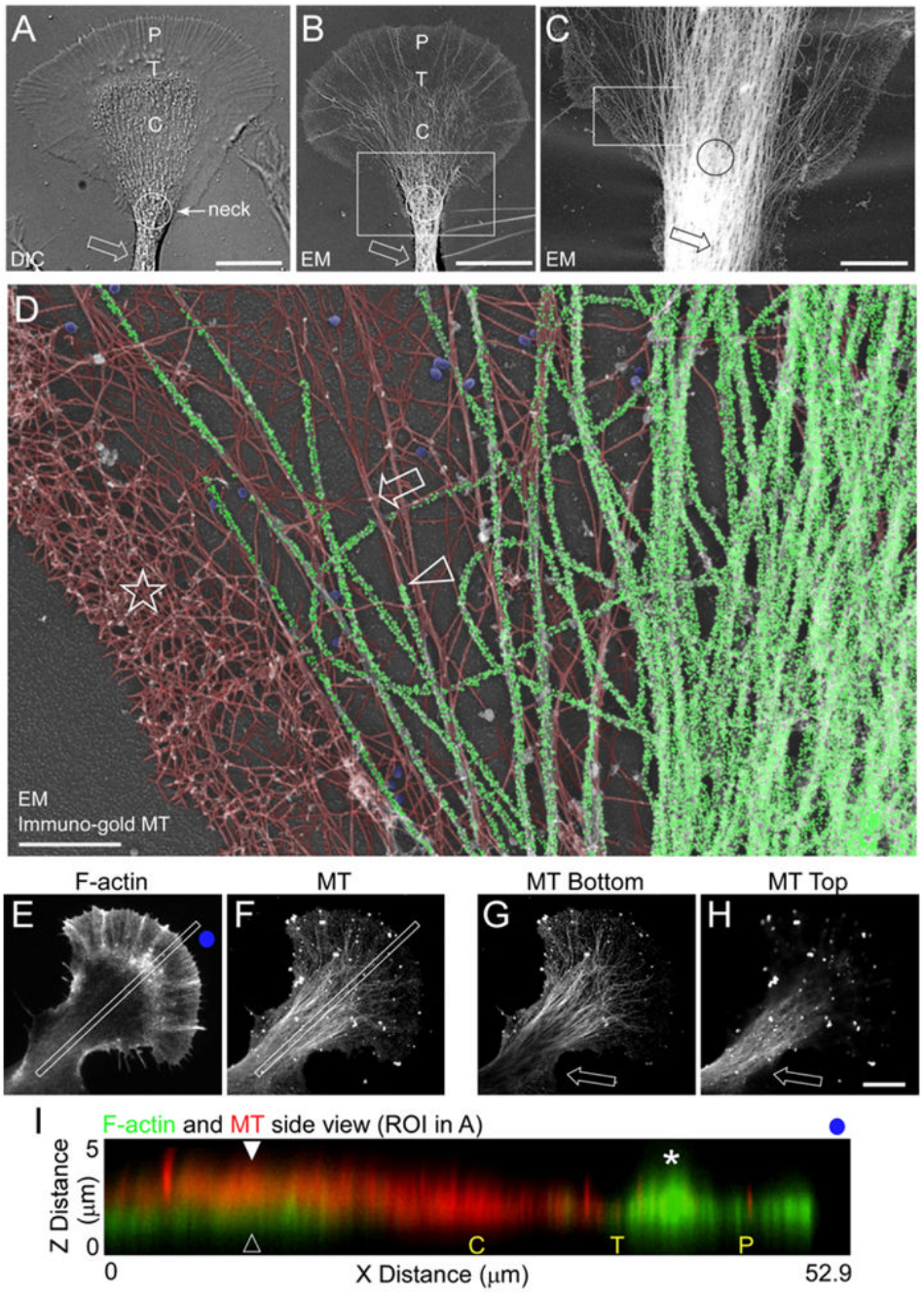

Figure 1. Individual MTs and Actin Filament Bundles Colocalize at the Growth Cone Neck

(A and B) Growth cone structural domains. DIC (A) and low-magnification EM (B) of two separate growth cones. P, T, and C denote peripheral domain, transition zone, and central domain, respectively. Circle denotes growth cone neck and arrow denotes neurite shaft.

(C) Gold-labeled MTs of a region similar to box in (B).

(D) Higher magnification of the box in (C). Star denotes actin network, arrow denotes an actin bundle, and arrowhead denotes a MT aligned with the actin bundle. Gold particles were individually pseudocolored green to denote MT localization. Actin filaments were pseudocolored red. Gold particle and actin filament labeling was performed with 100%

transparency and 22% transparency, respectively, using Canvas X. Clathrin vesicles are pseudocolored blue.

(E–H) Spinning disk confocal images of the F-actin and MT cytoskeletons. Full projection z section of the F-actin (E) and MT (F) z sections. Bottom (G) and top (H) view of the MTs.

(I) Overlay of the F-actin (green) and MT (red) kymographs taken from the regions of interest in (E) and (F). P, T, and C denote peripheral domain, transition zone, and central domain, respectively. Open arrowhead denotes the actin node and closed arrowhead denotes MTs above the actin node. Star denotes actin “ruffles” in the P domain. Blue dots in (E) and (F) give orientation. Scale bars: (A)–(B) and (E)–(H), 10 μm; (C), 5 μm; (D), 1 μm.

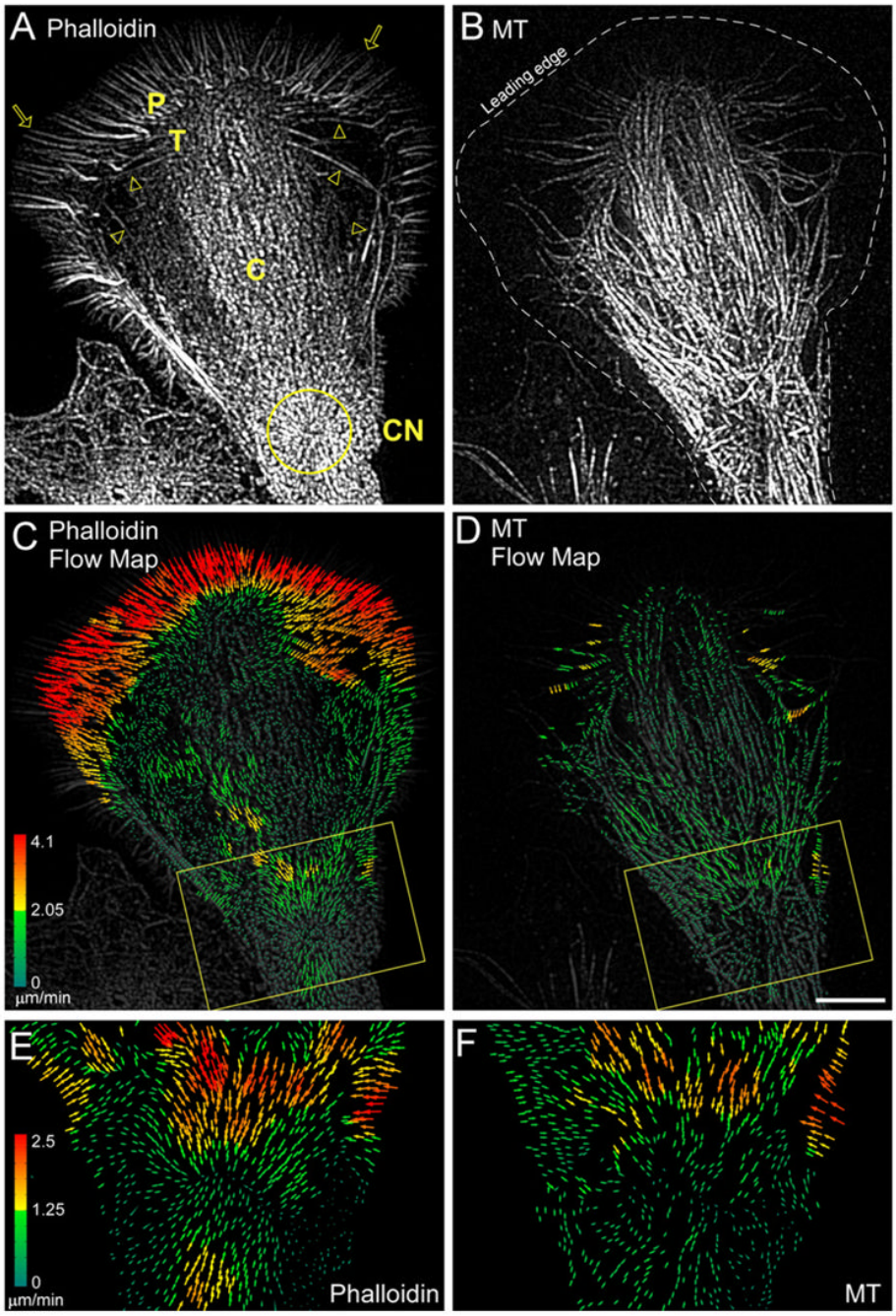

Figure 2. F-Actin and MTs Move Together into the Growth Cone Neck

(A and B) Fluorescent phalloidin (A) and MT (B) FSM in a growth cone.

(C and D) Corresponding flow maps for the phalloidin (C) and MT (D) channels. P, T, C, and CN denote peripheral domain, transition zone, central domain, and contractile node (yellow circle), respectively. Yellow boxes denote growth cone base.

(E and F) Yellow boxes in (C) and (D), respectively. Colors encode flow speed in μm min^{-1} and vector arrows, flow direction.

Scale bar, 10 μm.

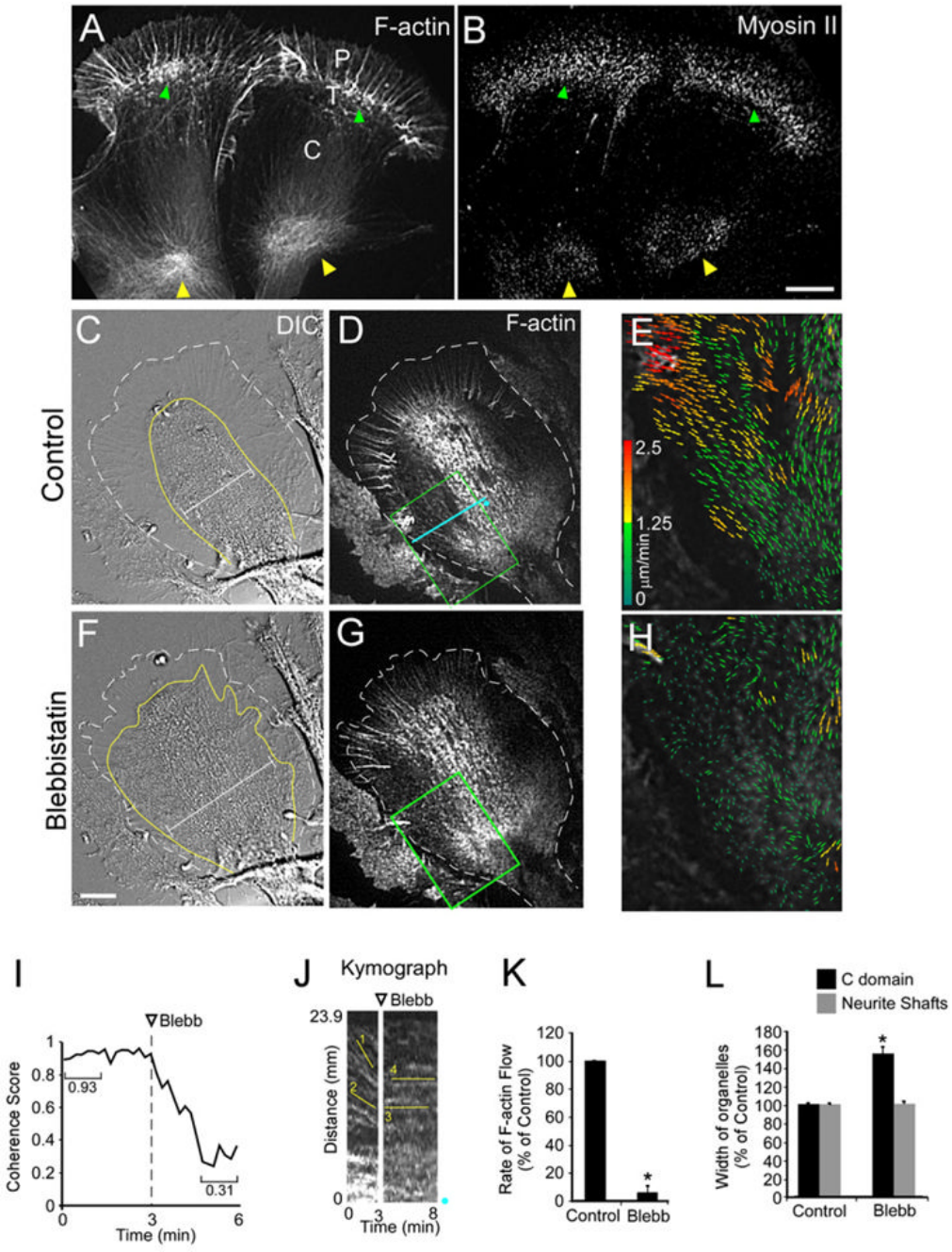

Figure 3. Myosin II Activity Drives Growth Cone Neck Actin Flow

(A and B) F-actin and Myosin II localized in two growth cones after live cell extraction. P domain, T zone, and C domain are labeled. Green arrowheads denote T zone and yellow arrowheads denote the actin node. Note myosin II localization in both regions (arrowheads in [B]).

(C–H) Blebbistatin slows actin flow in contractile node. DIC (C) and fluorescent phalloidin FSM (D) of a control growth cone. (E) F-actin FSM flow map of the box in (D). DIC (F) and fluorescent phallodin FSM (G) after 4 min in 70 µM blebbistatin. (H) Flow map of the box in (G). Dotted white lines in (C) and (F) denote leading edge of growth cone. Yellow lines denote

the C domain defined by the large organelle boundary, and calipers show the increase in C domain width after blebbistatin treatment.

(I) Flow coherence score before and after blebbistatin. The score is calculated by the magnitude of the vector mean of all normalized vectors in a sample box of 25 × 25 pixels ($1/N\sum Vi/|Vi,|$ ViVi/, normalized unit vector, N the number of vectors in the box) and calculating the magnitude of the vector mean. If the flow vectors in the box all point to the same direction, the score is 1. Otherwise if their directions are random, it is close to zero. The average score of all sample boxes covering the region of interest is shown.

(J) FSM kymograph from the blue line in (D). Blue dots show kymograph orientation. Lines denote flow before (1–2) and after (3–4) blebbistatin treatment.

(K) Flow rates slow down by 94.4 ± 4.5%.

(L) Organelle domain width in the C domain and neurite shafts before and 5–10 min after blebbistatin treatment (nine growth cones and eight neurite shafts, three measurements each). Width measurements taken perpendicular to the direction of growth cone extension.

Scale bars, 10 μm. * $p < 0.001$.

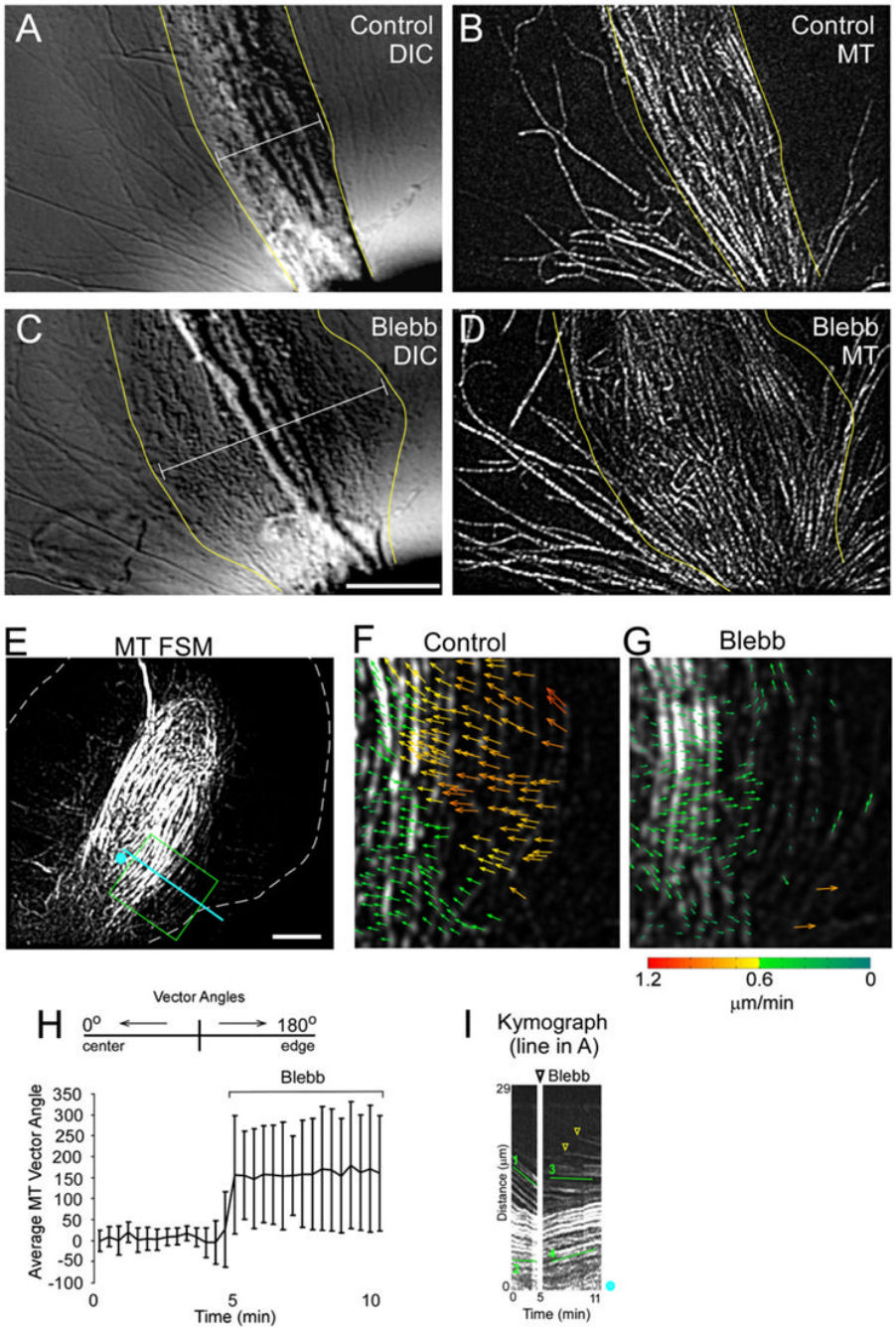

Figure 4. Myosin II Activity Bundles MTs into the C Domain

(A–D) Result of blebbistatin treatment on MT and organelle distributions. DIC (A) and MT FSM (B) of a control growth cone. DIC (C) and MT FSM (D) after 8 min in 70 μM blebbistatin. Yellow lines denote the C domain and calipers show the increase in width after blebbistatin treatment.

(E–G) MTs stop moving into the middle of the neck after blebbistatin treatment. (E) MT FSM of control growth cone. (F and G) Flow map from the box in (E) before (F) and 6 min after (G) blebbistatin treatment.

(H) Average vector angles in the middle of the neck before and after blebbistatin. Error bars show standard deviation.

(I) MT FSM kymograph from the line in (A). Lines 1 and 2 denote control fast and slow MT flow, respectively. Lines 3 and 4 denote the same regions as 1 and 2, respectively, after blebbistatin treatment. Note the fast MTs on the side stop almost instantaneously (line 3), and the MTs in the C domain start spreading out. Arrowheads denote new MTs passing the kymograph line.
Scale bars, 10 μm.